Small Angle Neutron Scattering Study of Microstructural Transitions in a Surfactant-Based Gel Mesophase

Blake A. Simmons,[†] Glen C. Irvin,[†] Vivek Agarwal,[‡] Arijit Bose,[‡] Vijay T. John,*[,†] Gary L. McPherson,*[,§] and Nitash P. Balsara[||]

Department of Chemical Engineering and the Department of Chemistry, Tulane University, New Orleans, Louisiana 70118, the Department of Chemical Engineering, University of Rhode Island, Kingston, Rhode Island 02881, and the Department of Chemical Engineering, University of California at Berkeley, Berkeley, California 94720

Received October 9, 2001

A surfactant-based rigid gel mesophase containing bis(2-ethylhexyl) sodium sulfosuccinate (AOT), phosphatidylcholine (lecithin), 2,2,4-trimethylpentane (isooctane), and D_2O has been characterized using small angle neutron scattering (SANS). The addition of water to a solution of AOT and lecithin in isooctane leads to a dramatic increase in viscosity and the formation of a rigid gel as the water content is increased above a specific threshold. SANS profiles indicate that these gels have a crystalline microstructure with characteristic dimensions that are clearly correlated to the system's water content and temperature. The scattering patterns are consistent with models that describe the microstructure as columnar hexagonal at lower water contents and temperatures and lamellar at higher water contents and temperatures. SANS is also able to examine characteristics of the intermediate region where the two phases coexist and to calculate the characteristic dimensions of these microstructures. The rigidity of the gel indicates that the system may be useful in templated materials synthesis.

Introduction

Microemulsions are systems that are composed of oil, water, and an amphiphilic surfactant. When thoroughly mixed, these components form a thermodynamically stable, isotropic solution.[1] These microstructures may take the form of lamellar layers of oil and water,[2] well-defined spherical droplets or cylinders of one phase dispersed throughout a bulk phase,[3] intercontiguous networks,[4] or disordered/ordered bicontinuous networks of both phases.[5,6] In all of these microstructures, the surfactants form a stable amphiphilic layer that separates the aqueous and organic phases into well-defined, observable domains.[7]

The twin-tailed anionic surfactant bis(2-ethylhexyl) sodium sulfosuccinate (AOT), shown in Figure 1a, typically forms water-in-oil microemulsions.[8] AOT has a surfactant packing parameter, P, of 1.1 ($P = v/al$, where v is the volume occupied by the tails, a is the effective headgroup cross-sectional area, and l is the maximum effective tail length) and tends to have a spontaneous curvature that is concave toward water.[9,10] These macroscopically single-phase water-in-oil microemulsions can incorporate water typically to a water/AOT level (W_0 is defined as the water/AOT molar ratio) of 30−40. The zwitterionic surfactant phosphatidylcholine (lecithin), shown in Figure 1b, has a significantly larger headgroup and a smaller packing parameter of 0.6 than does AOT.[9,11] In aqueous systems, lecithin tends to form interfaces with mimimal curvatures,

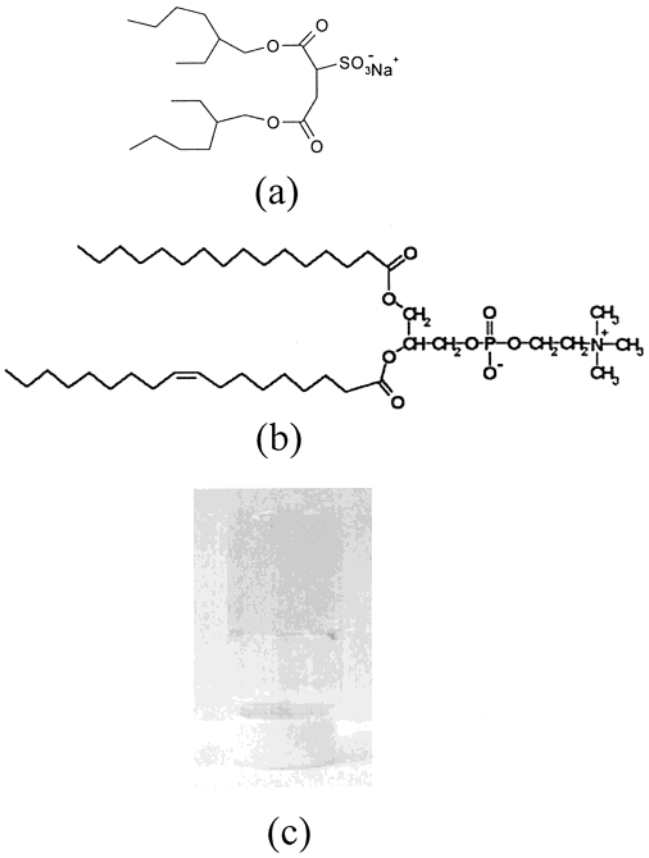

Figure 1. Chemical structures of (a) the anionic surfactant bis(2-ethylehxyl) sulfosuccinate (AOT) and (b) the zwitterionic phospholipid phosphatidylcholine (lecithin). (c) Photograph of a $W_0 = 90$ gel at ambient conditions.

* Corresponding authors. E-mail: vijay.john@tulane.edu or garym@tulane.edu.
[†] Department of Chemical Engineering, Tulane University.
[‡] University of Rhode Island.
[§] Department of Chemistry, Tulane University.
[||] University of California at Berkeley.

(1) Daniellson, A.; Lindman, B. *Colloids Surf.* **1981**, *3*, 391.
(2) Huh, C. *J. Colloid Interface Sci.* **1979**, *71*, 408.
(3) Lagues, M.; Ober, R.; Taupin, C. *J. Phys., Lett.* **1978**, *39*, L-487.
(4) De Geyer, A.; Tabony, J. *Chem. Phys. Lett.* **1985**, *113*, 83.
(5) Jouffray, J.; Levinson, P.; De Gennes, P. G. *J. Phys.* **1982**, *43*, 1241.
(6) Kaler, E. W.; Bennet, K. E.; Davis, H. T.; Scriven, L. E. *J. Chem. Phys.* **1983**, *79*, 5673.
(7) Lichterfeld, F.; Schmeling, T.; Strey, R. *J. Phys. Chem.* **1986**, *90*, 5762.
(8) Kotlarchyk, M.; Stephens, R. B.; Huang, J. S. *J. Phys. Chem.* **1988**, *92*, 1533.
(9) Israelachvili, J. N. *Intermolecular and Surface Forces*; Academic Press: New York, 1992.
(10) De, T. K.; Maitra, A. *Adv. Colloid Interface Sci.* **1995**, *59*, 193.

10.1021/la011530r CCC: $22.00
Published on Web 01/11/2002

such as flexible bilayers and vesicles.[9] In nonpolar solvents, lecithin forms wormlike cylindrical reverse micelles that can incorporate water up to a water/lecithin molar ratio of 20.[12] In a series of papers by Luisi and co-workers,[12] it was shown that the entanglements of these wormlike micelles lead to viscous gels with zero shear viscosities as high as 10^3 Pa·s at optimal water content.

This work is based on our finding that the combination of AOT and lecithin leads to a highly rigid gel that can incorporate significantly high water content.[13] For example, when AOT and lecithin are dissolved in isooctane at concentrations of 0.8 and 0.4 M, respectively, the solution follows Newtonian behavior with a low viscosity of 0.1 Pa·s. When water is added to the system, the viscosity increases, and the solution turns to a rigid gel phase when $W_0 = 50-70$. The gel stays rigid for W_0 levels of up to 200, and typical zero shear viscosities over this range are on the order of 10^6 Pa·s.[13] Thus, these surfactant gels may be sufficiently rigid to serve as templates for the synthesis of nanostructured materials, where the spatial immobilization of the hydrophobic and the hydrophilic regions would allow the formation of extended structures that are organized over multiple length scales.

To exploit these systems for templated synthesis from the fundamental perspective of self-assembly in mixed surfactant systems, it is important to understand the microstructure of the gel phase. In the current study, we report the results of small angle neutron scattering studies (SANS) of these gels over a range of water content. Over the past several years, small angle neutron scattering (SANS) studies of different microemulsion systems have been carried out, and the results have led to a better understanding of their existing microstructures and phase-transition behavior.[14] Water-in-oil microemulsions of AOT have been extensively characterized by numerous methods, including SANS.[8] The elucidation of the wormlike micelles of lecithin in organic solvents and the entanglements of these structures to form gels have also been studied extensively using SANS.[15]

As described in the following sections, SANS analysis is useful in elucidating the gel microstructure at various water content and temperature values. In addition, we find that SANS is very useful in characterizing the evolution of one microstructure to another and is able to identify transitional states between these microstructures.

Experimental Section

Chemicals. Lecithin (95% purity) extracted from soybeans was obtained from Avanti Polar Lipids, Inc. Bis(2-ethylhexyl) sodium sulfosuccinate (AOT) and 2,2,4-trimethylpentane (isooctane, 99% purity) were purchased from Sigma. Deuterium oxide (99.9%) was purchased from Cambridge Isotopes Laboratory. All chemicals were used without further treatment or purification.

Table 1. Sample Compositions[a]

W_0	D_2O (mL)	D_2O (g)	α_{aq}	α_s	α_o	φ_w	φ_s	φ_o
70	5.368	5.959	0.462	0.270	0.268	0.450	0.131	0.419
90	6.902	7.661	0.525	0.238	0.237	0.513	0.116	0.371
110	8.436	9.364	0.574	0.213	0.212	0.562	0.104	0.333
130	9.970	11.067	0.615	0.193	0.192	0.602	0.095	0.303
150	11.504	12.769	0.648	0.177	0.176	0.637	0.087	0.277
170	13.038	14.472	0.676	0.163	0.162	0.665	0.080	0.255

[a] Composition of each W_0 is based on 0.85 M AOT (1.89 g) and 0.42 M lecithin (1.59 g) dissolved in 5 mL of isooctane. α_{aq}, α_s, and α_o denote the weight fractions of the aqueous phase, both surfactants (AOT and lecithin), and the oil phase, respectively. φ_{aq}, φ_s, and φ_o denote the corresponding volume fractions of the aqueous phase, both surfactants (AOT and lecithin), and the oil phase, respectively. In translating experimental weight fractions to volume fractions, an effective surfactant density of 2.2 g/mL was assumed.

Samples. Typical compositions of the rigid gel mesophases containing lecithin and AOT were prepared by synthesizing 0.85 M AOT (1.89 g) and 0.42 M lecithin (1.59 g) solutions in 5 mL of isooctane. These solutions were sonicated in a warm water (38 °C) bath until completely homogeneous, clear yellow liquid was formed. Solution compositions were fixed for all of the systems analyzed so that the effect that the increasing water content had upon the mesophase and its subsequent microstructure could be determined. D_2O was added in incremental measured quantities (ca. 0.5 mL per increment) to obtain the desired W_0 ($W_0 = [D_2O]/[AOT]$) = 70, 90, 110, 130, 150, and 170). After the D_2O was added, the samples were sonicated in a warm water bath and vortexed until a clear yellow liquid was obtained. This process was repeated until the total required amount of D_2O was added for the corresponding W_0 value. The samples were then removed from the water bath and allowed to cool to ambient temperature. The $W_0 = 70$ system is at the gelation threshold and is in a "soft" gel phase. Rigid gel mesophases formed at $W_0 \geq 90$ were isotropic, transparent, and slightly yellow in color.

SANS measurements were carried out on the 30 m NG3 beam line at the National Institute for Standards and Technology (NIST) Center for Neutron Research (NCNR) in Gaithersburg, MD. The SANS intensity, I_q, was recorded as a function of the scattering vector q ($q = 4\pi \sin(\theta/2)/\lambda$ with θ defined as the scattering angle and λ, as the neutron wavelength). The neutron wavelength used for this study was 6 Å. The detector angle was set at 2°, and the sample-to-detector distance was set to 6 m. The range of the scattering vector q was $0.007-0.1039$ Å^{-1}. Samples were contained in closed stainless steel cells with quartz windows that provided a path length of 2 mm. The temperature was controlled using the 10-position sample changer (−10 to 90 °C) provided by NCNR. The temperature was raised in increments of 15 °C over a setpoint range of 25−70 °C. The samples were allowed to equilibrate at each temperature for 1 h before the SANS data was acquired. At the higher temperatures, there is an offset between the setpoint temperature and the actual temperature in the cell. We report the data in terms of the actual temperatures (25, 38, 52, and 65 °C). After the run at 65 °C was completed, the temperature was lowered to 25 °C. The samples were then allowed to cool for 2 h at 25 °C to ensure that thermal equilibrium was attained. Following this process, another set of SANS measurements was made to determine if these systems were thermally reversible. The SANS data were corrected for empty-cell scattering, detector sensitivity, and background scattering. A NIST secondary standard was used to obtain absolute scattering intensities (cm^{-1}).

Results and Discussion

General Characteristics of the Scattering Patterns. The compositions of the samples used in this study are listed in Table 1. At ambient temperature, the $W_0 = 70$ system is an incipient gel and is somewhat softer than the rigid gels formed at higher W_0 values. Figure 2a illustrates the results of SANS measurements for $W_0 = 70-170$ at 25 °C. In all samples, the scattering results

(11) Wabel, C. Ph.D. Dissertation, University of Erlangen, 1998.
(12) Scartazzini, R.; Luisi, P. L. *J. Phys. Chem.* **1988**, *92*, 829. Capitani, D.; Segre, A. L.; Sparapani, R.; Giustini, M.; Scartazzini, R.; Luisi, P. L. *Langmuir* **1991**, *7*, 250. Schurtenbergere, P.; Scartazzini, R.; Luisi, P. L. *Rheol. Acta* **1989**, *28*, 372. Luisi, P. L.; Scartazzini, R.; Haering, G.; Schurtenberger, P. *Colloid Polym. Sci.* **1990**, *268*, 356.
(13) Li, S.; Irvin, G. C.; Simmons, B.; Rachakonda, S.; Ramannair, P.; Banerjee, S.; John, V. T.; McPherson, G. L.; Zhou, W.; Bose, A. *Colloids Surf., A* **2000**, *174*, 275.
(14) Chen, S. H.; Choi, S. M. *Supramol. Sci.* **1998**, *5*, 197. Teubner, M.; Strey, R. *J. Chem. Phys.* **1987**, *90*, 5672. Choi, S. M.; Chen, S. H.; Sottmann, T.; Strey, R. *Physica B* **1998**, *241−243*, 976. Subramanian, G.; Hjelm, R. P.; Deming, T. J.; Smith, G. S.; Li, Y.; Safinya, C. R. *J. Am. Chem. Soc.* **2000**, *122*, 26. Bergstrom, M.; Pedersen, J. S.; Salamat, G.; de Vries, R.; Kaler, E. W.; Satija, S.; Sung, L. *Langmuir* **2000**, *16*, 102.
(15) Schurtenberger, P.; Magid, L. J.; King, S. M.; Lindner, P. *J. Phys. Chem.* **1991**, *95*, 4173. Schurtenberger, P. *Chimia* **1994**, *48*, 72. Schurtenberger, P.; Cavaco, C. *Langmuir* **1994**, *10*, 100.

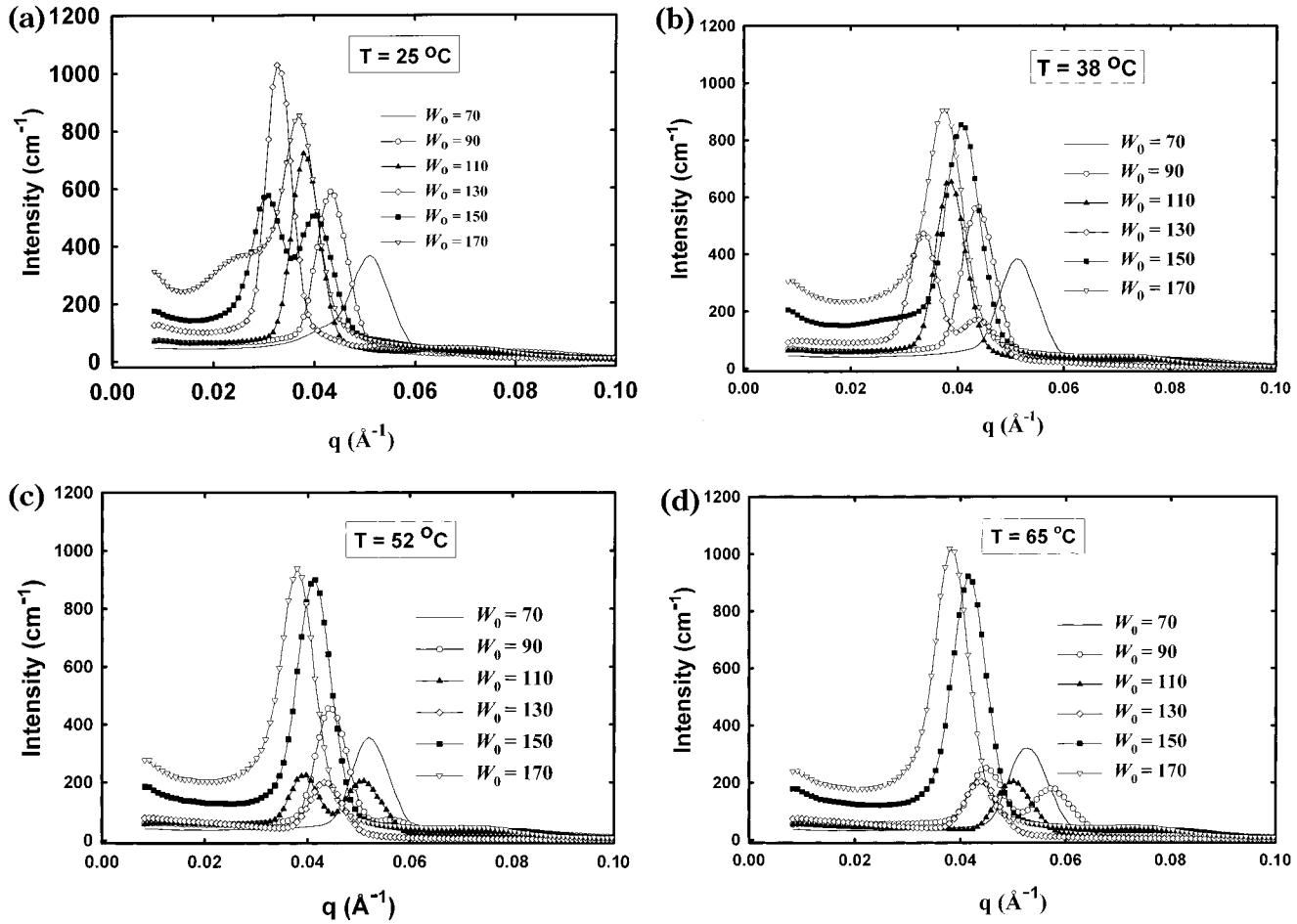

Figure 2. SANS data on a linear scale from $W_0 = 70$, 90, 110, 130, 150, and 170 systems analyzed at (a) 25, (b) 38 , (c) 52, and (d) 65 °C.

show the presence of at least one strong peak at $q = q_m$, indicative of a periodic structure. If we follow the scattering trends from $W_0 = 70$ to 130, we observe a shift of this peak to lower q values. For the rigid gel systems at $W_0 = 90$, 110, and 130, q_m decreases in steps of about 0.005 Å^{-1}. The decrease in the q value is due to a "swelling" effect in the aqueous domain size. From the relationship $q = 2\pi/d$, the decrease in q_m translates to an increase of ca. 20 Å in the characteristic repeat distance, d, between aqueous domains for each increment of 20 in W_0.

When the W_0 value is further increased to 150, we observe the emergence of two peaks (Figure 2b). The dominant peak, q_m, occurs at 0.031 Å^{-1} and follows the trend described above (the difference in q_m between the $W_0 = 130$ and 150 rigid gel mesophases is ca. 0.002 Å^{-1}). The second peak, q_s, occurs at a higher q of 0.041 Å^{-1}. The fact that the intensities of the q_s and q_m peaks are similar strongly suggests the presence of two coexisting microstructures. Two coexisting microstructures are also seen in the $W_0 = 170$ sample, but they are shifted to smaller q values with a reversal in intensities. There is a strong peak at 0.037 Å^{-1} and a broad shoulder centered at 0.027 Å^{-1}. Comparing the $W_0 = 150$ and 170 systems, the shift in the dominant-peak q_m values implies that a transition from one microstructure to another occurs after a critical W_0 value has been reached. Overall, there is also an increase in peak intensity with water content. The intensity of a scattering peak is a function of the order in the system, the concentration of D_2O, and the instrument resolution. While intensity increases are typically associated with an increase in enhanced ordering, we note here that as W_0 increases, the concentration of the scattering element (D_2O) also increases and contributes to the observed increase in integrated intensity.

Figure 2b–d illustrates the scattering patterns for the samples at 38, 52, and 65 °C, respectively. Figure 2b at 38 °C has very similar scattering characteristics to Figure 2a. There is a shift to lower q_m as the water content is increased from $W_0 = 70$ to 110. At $W_0 = 130$, peak splitting is again observed, and there is a broadening of the peaks attributed to a loss of long-range correlation in the system. Again, there appears to be some softening of the gel at $W_0 = 130$. With further increases in W_0 to 150 and 170, the system regains the characteristics of a rigid gel. Highly resolved peaks are observed, indicating that long-range order has been regained. We see similar trends at the higher temperatures (Figure 2c and d).

The key scattering features that lead us to an understanding of the microstructure are the weak higher-order peaks, q_{ho}, occurring at higher q values in Figure 2a–d. These higher-order features are clearly evident in many samples when the data are plotted on a logarithmic scale. Two examples ($W_0 = 90$ and 170 at 25 and 52 °C, respectively) of this behavior are shown in Figure 3. In the first case, q_{ho} is 0.076 Å^{-1} while q_m is 0.043 Å^{-1}. The value of q_{ho} is $\sqrt{3}\,q_m$, which is a classic signal of scattering from a columnar hexagonal phase. Thus, q_m is due to diffraction from the [1,0] reflections that connect nearest neighbors in a columnar hexagonal lattice while q_{ho} is due to diffraction from the [1,1] reflections that connect second nearest neighbors.[16] The d-spacings of the [1,0] reflections

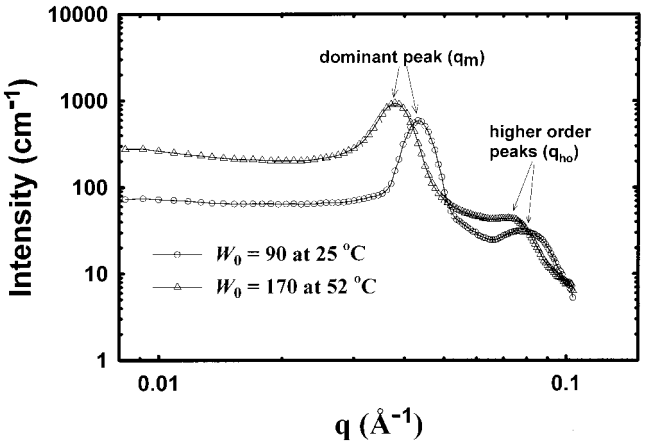

Figure 3. Log−log plot of the SANS data from the $W_0 = 90$ and 170 gels at 25 and 52 °C, respectively, showing the higher-order features at higher q values.

Table 2. Peak Positions as a Function of Temperature for Each W_0[a]

W_o	T (°C)	system appearance	q_m (Å^{-1})	q_s (Å^{-1})	q_{ho} (Å^{-1})	$\sqrt{3}\ q_m$ (Å^{-1})	$2q_m$ (Å^{-1})
70	25	gel	0.051	0.042	0.087	0.088	0.102
	38	gel	0.051				
	52	gel	0.052				
	65	gel	0.053				
	25r	gel	0.051	0.043	0.081	0.088	0.102
90	25	gel	0.043		0.076	0.075	0.086
	38	gel	0.044		0.076	0.076	0.088
	52	gel	0.044	0.055	0.080	0.076	0.088
	65	visc. liq.	0.045	0.057			
	25r	gel	0.043		0.075	0.075	0.086
110	25	gel	0.038		0.068	0.066	0.076
	38	gel	0.039		0.068	0.067	0.078
	52	visc. liq.	0.040	0.051			
	65	visc. liq.	0.050				
	25r	gel	0.038		0.066	0.066	0.076
130	25	gel	0.033		0.054	0.057	0.065
	38	visc. liq.	0.034	0.044			
	52	visc. liq.	0.043				
	65	gel	0.044		0.081	0.076	0.088
	25r	gel	0.033		0.057	0.057	0.065
150	25	gel	0.031	0.041	0.077	0.054	0.062
	38	visc. liq.	0.041	0.032	0.078	0.070	0.081
	52	gel	0.041		0.079	0.072	0.083
	65	gel	0.041		0.077	0.072	0.083
	25r	gel	0.031	0.040	0.080	0.054	0.062
170	25	gel	0.037	0.027	0.068	0.064	0.074
	38	gel	0.038		0.072	0.066	0.076
	52	gel	0.038		0.072	0.066	0.076
	65	gel	0.038		0.072	0.066	0.076
	25r	gel	0.037	0.027	0.072	0.064	0.074

[a] q_m, q_s, and q_{ho} are the dominant, secondary, and higher-order peaks from the data, respectively. Empty table entries indicate that there was no detectable feature in the corresponding SANS data. The entry "25r" indicates a return to 25 °C after heating to 65 °C.

are $\sqrt{3}$ times the d-spacings of the [1,1] planes. In the second case, the value of q_{ho} is $2q_m$ and is a signature of scattering from a lamellar phase; this term arises simply from the harmonic ($n = 2$) in Bragg's equation. Thus, the two higher-order features enable distinctions between the hexagonal and lamellar phases to be made.

Table 2 summarizes all the above observations and lists all the higher-order features observed. q_m in Table 2 refers to the dominant peak, q_s refers to the second feature that is observed in the microstructure coexistence stage, and q_{ho} refers to the higher-order features detected at higher q values. Also listed in Table 2 are values of the higher-order peaks that correspond to hexagonal or lamellar symmetry ($\sqrt{3}\ q_m$ and $2q_m$, respectively); the agreement between the observed higher-order peaks and those calculated from q_m serves as an indication of the system's microstructure. The data in Table 2 indicate that there is a transition through a coexistence region that occurs when each system moves from one phase to another as the temperature is increased, as required by the Gibbs phase rule.[17,18] A good example of this transition is found in the $W_0 = 130$ system. At 25 °C, $q_m = 0.0327$ Å^{-1} with no q_s present. The agreement of q_{ho} with $\sqrt{3}\ q_m$ indicates that the system has hexagonal symmetry. At 38 °C, there is the appearance of a q_s at 0.044 Å^{-1} and the q_m has increased to 0.0336 Å^{-1}; these features are evidence of the coexistence of the two microstructures. At 52 °C, a shift in the peaks is observed, with the previous q_s now becoming the q_m. At 65 °C, the system reverts to the rigid gel mesophase, and the q_m remains virtually unchanged. Also at 65 °C, the higher-order feature at $q_{ho} = 0.081$ Å^{-1} has moved toward the q value that would be obtained from a lamellar microstructure. As a final observation, the thermal reversibility of the system is illustrated by the data denoted at 25r, which is obtained by bringing the system back to ambient temperature (Table 2).

This phenomenon of the emergence of a secondary peak, q_s, with an increase in the temperature and the subsequent replacement of the original q_m is repeated in one form or another for the systems at $W_0 = 110$, 130, and 150. We interpret this behavior as a transformation from a hexagonal microstructure to a lamellar microstructure with increasing temperature. With the $W_0 = 70$ system, the indication is that the transformation has not yet occurred at 65 °C. With $W_0 = 150$, the indication is that the system is already in the microstructure coexistence stage at 25 °C, and further increases in temperature bring it into the lamellar region.

Microstructure Analysis. While the above qualitative interpretations are based on the observations of scattering patterns, the microstructure transitions and the individual peak positions can be predicted by analysis of the underlying geometries of the hexagonal and lamellar microstructures.

A 2-D cross-sectional schematic of the proposed columnar hexagonal microstructure is presented in Figure 4a. In this microstructure depiction, we assume that the water phase consists of cylindrical tubes packed in hexagonal symmetry, which is the representation of the inverted hexagonal phase (H_{II}).[19] The cross-sectional area of the unit cell (A_{uc}) is

$$A_{uc} = 2a^2\sqrt{3} \quad (1)$$

where $2a$ is defined as the center-to-center distance between aqueous cores. The experimentally observed d-spacing is related to a through

$$d = a\sqrt{3} \quad (2)$$

(16) Cullity, B. D. *Elements of X-ray Diffraction*; Addison-Wesley: Reading, MA, 1975.

(17) Laughlin, R. G. *The Aqueous Phase Behavior of Surfactants*; Academic Press: London, 1994; p 82.

(18) Lee, J. H.; Balsara, N. P.; Krishnamoorti, R.; Jeon, H. S.; Hammouda, B. *Macromolecules* **2001**. In press.

(19) Evans, D. F.; Wennerstrom, H. *The Colloidal Domain*; Wiley-VCH: New York, 1999.

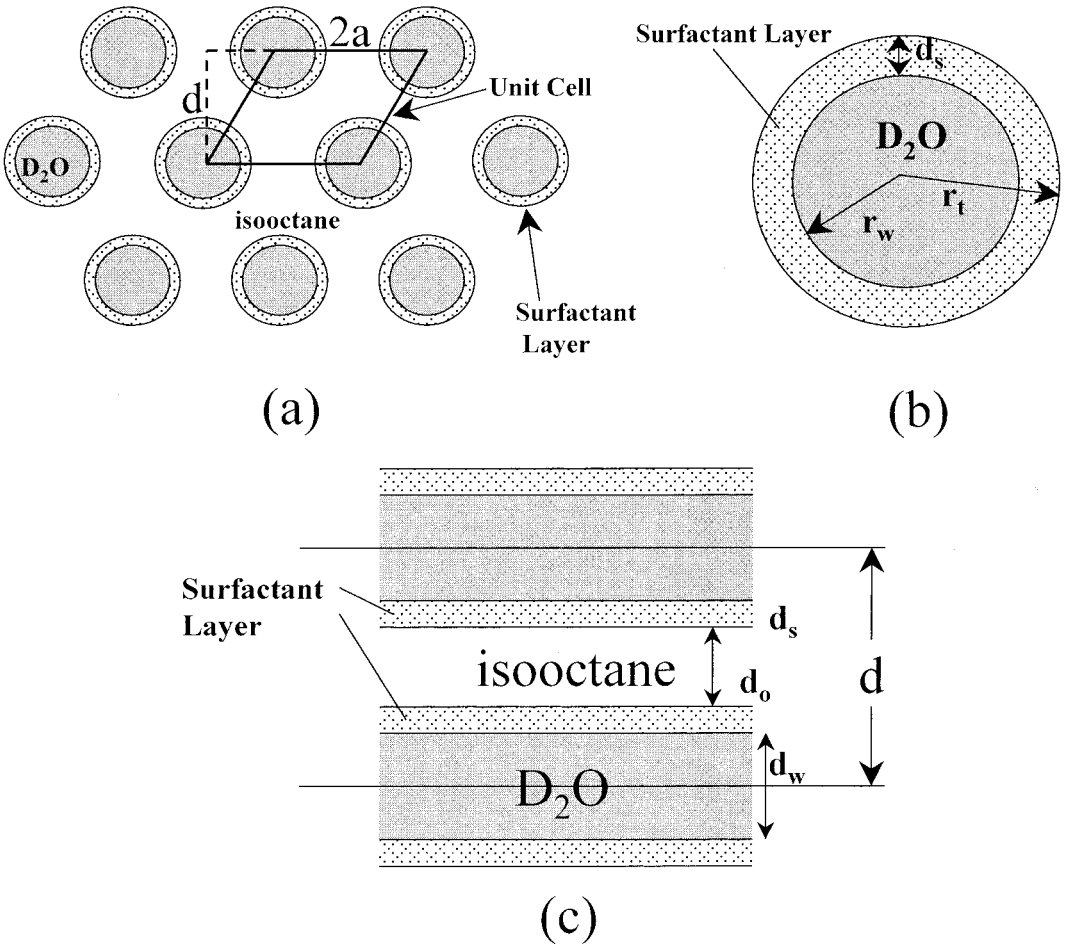

Figure 4. Schematics depicting (a) the geometry of the hexagonal microstructure, (b) the size parameters within a single cylinder of the hexagonal microstructure, and (c) the geometry of the lamellar microstructure.

The unit cell cross-sectional area is made up of contributions from the water, oil, and surfactant components.

$$A_{uc} = A_w + A_s + A_o \tag{3}$$

where A_w is the area of the aqueous phase, A_s is the area of the surfactants, and A_o is the area of the oil phase. An enlarged view of one of the water cylinders with the amphiphile layer is shown in Figure 4b. In columnar hexagonal geometry, the volume fractions of the three components are identical to the cross-sectional area fractions. It follows that the area of the inner aqueous core can be described by

$$A_w = \pi r_w^2 = 2a^2 \varphi_w \sqrt{3} \tag{4}$$

where r_w is the radius of the aqueous phase and φ_w is the aqueous-phase volume fraction. Similarly,

$$A_w + A_s = \pi r_t^2 = 2a^2(\varphi_w + \varphi_s)\sqrt{3} \tag{5}$$

Combining eqs 4 and 5 leads to

$$\frac{r - r_w}{a} = \frac{d_s}{a} = \left(\sqrt{\frac{2\sqrt{3}}{\pi}}\right)(\sqrt{\varphi_w + \varphi_s} - \sqrt{\varphi_w}) \tag{6}$$

where d_s is the thickness of the surfactant layer.

For the lamellar (L_α) arrangement depicted in Figure 4c, there are alternating layers of water and oil phases each separated by a surfactant layer of a constant thickness. Thus,

$$d = 2d_s + d_w + d_o \tag{7}$$

where d_s is the thickness of the surfactant layer, d_o is the thickness of the oil layer, and d_w is the thickness of the aqueous layer. Again, using the fact that in the lamellar system the fractional thicknesses of the various layers are proportional to their volume fractions, we can write

$$d = \frac{2d_s}{\varphi_s} \tag{8}$$

Equations 6 and 8 allow us to calculate the peak locations ($d = 2\pi/q_m$) given the system composition (volume fractions) and an effective surfactant thickness layer d_s. It is possible to use the experimental data for systems clearly in the lamellar region to obtain d_s from a regression of eq 8 rearranged to

$$d = \frac{2\pi}{q_m} = \frac{2d_s}{V_S}(V_s + V_o + V_w) = 2d_s + \frac{2d_s}{V_s}(V_o + V_w) \tag{9}$$

Thus, a plot of $2\pi/q_m$ versus $(V_o + V_w)$ (i.e., changing V_w or W_o at constant oil and surfactant contents) should be linear over the lamellar region, and d_s can be obtained from the intercept. We used the experimental data at 65 °C and W_o = 110, 130, 150, and 170, where the system shows lamellar behavior, to carry out the regression. The

Table 3. Comparison of Experimental and Predicted q_m Values for the Hexagonal and Lamellar Microstructures at Each W_0[a]

W_0	T (°C)	q_m (Å^{-1})	q_s (Å^{-1})	$q_{m,p}{}^h$ (Å^{-1})	$q_{m,p}{}^l$ (Å^{-1})	structure
70	25	0.051	0.042	0.051	0.060	hexagonal
	38	0.051		0.051	0.060	hexagonal
	52	0.052		0.051	0.060	hexagonal
	65	0.053		0.051	0.060	hexagonal
	25r	0.051	0.043	0.051	0.060	hexagonal
90	25	0.043		0.043	0.053	hexagonal
	38	0.044		0.043	0.053	hexagonal
	52	0.044	0.055	0.043	0.053	coexisting
	65	0.045	0.057	0.043	0.053	coexisting
	25r	0.043		0.043	0.053	hexagonal
110	25	0.038		0.037	0.048	hexagonal
	38	0.039		0.037	0.048	hexagonal
	52	0.040	0.051	0.037	0.048	coexisting
	65	0.050		0.037	0.048	lamellar
	25r	0.038		0.037	0.048	hexagonal
130	25	0.033		0.032	0.043	hexagonal
	38	0.034	0.044	0.032	0.043	coexisting
	52	0.043		0.032	0.043	lamellar
	65	0.044		0.032	0.043	lamellar
	25r	0.033		0.032	0.043	hexagonal
150	25	0.031	0.041	0.029	0.039	coexisting
	38	0.041		0.029	0.039	lamellar
	52	0.041		0.029	0.039	lamellar
	65	0.041		0.029	0.039	lamellar
	25r	0.031	0.040	0.029	0.039	coexisting
170	25	0.037	0.027	0.026	0.036	coexisting
	38	0.038		0.026	0.036	lamellar
	52	0.038		0.026	0.036	lamellar
	65	0.038		0.026	0.036	lamellar
	25r	0.037	0.027	0.026	0.036	coexisting

[a] q_m and q_s are the dominant and secondary peak positions obtained from the data, respectively. $q_{m,p}{}^h$ and $q_{m,p}{}^l$ values are predictions of the q_m value and are based on either a hexagonal or lamellar microstructure, respectively. Missing table elements imply that there was no corresponding peak or feature present in the SANS data.

regression analysis yielded $d_s = 6.9$ Å and $V_s/V_o = \phi_s/\phi_o = 0.31$ with a regression coefficient of 0.985. An effective surfactant density calculated from these volume fractions is 2.2 g/mL, indicating significantly tight surfactant packing. Experimental surfactant densities obtained by measuring the volume change associated with the addition of surfactant are in the range 2.1−2.5 g/mL, but these measurements are subject to wide variations in the gel phase. In subsequent calculations, we have used the value of $d_s = 6.9$ Å for both lamellar and hexagonal microstructures. This value for the surfactant layer thickness is considerably below the range of the geometric length scale of lecithin tails, but it is reasonably close to the 9 Å tail length reported for AOT in reverse micelles.[20] Perhaps the calculation reflects a dominating influence of AOT at the 2:1 AOT/lecithin composition and might also represent the thickness of the surfactant shell that is completely impervious to D_2O. We do not at present ascribe a molecular interpretation to the value of d_s and simply state that it represents an effective surfactant layer thickness that is consistent with the models.

The results of the hexagonal and lamellar models are presented in Table 3 and illustrate very good agreement between the observed q_m values and either the hexagonal or lamellar microstructure calculations. When both q_m and q_s are observed, there is agreement of one feature with the hexagonal microstructure calculation and of the other with the lamellar microstructure calculation. For example, if we follow the systems at 38 °C, we see that at $W_0 = 70$ the system has a columnar hexagonal microstructure. At $W_0 = 130$, we observe the coexistence state that has both hexagonal and lamellar symmetry. At $W_0 = 150$, the system shifts entirely to the lamellar microstructure, which is retained at $W_0 = 170$. Conversely, we can follow the temperature profiles at a specific W_0 (e.g., 130) and observe the transition from the hexagonal to the lamellar microstructure with increasing temperature. Thus, there is a transition from the hexagonal to the lamellar microstructure that depends on both water content and temperature.

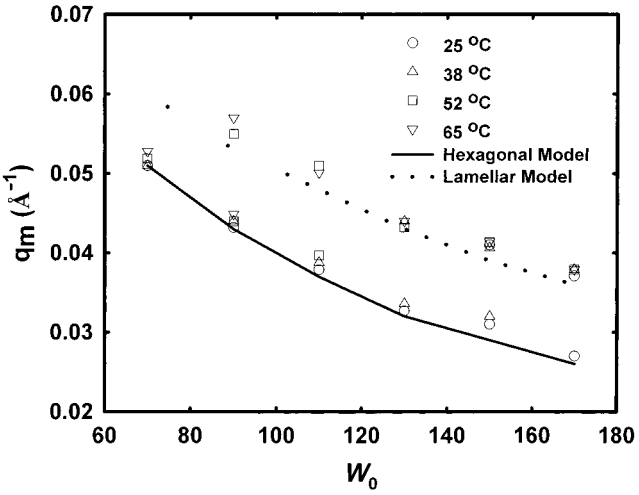

Figure 5. Graph of peak positions q_m and q_s vs W_0 as a function of temperature, indicating the transition in microstructure that occurs as a function of W_0 and temperature. The presence of two ordinate values for a single W_0 at a given temperature indicates the presence of both dominant and secondary features in the SANS data. The curves are predictions based on lamellar and hexagonal microstructures.

The experimental and predicted peak locations are summarized in Figure 5. There are two obvious trend lines present in the data, each one representing a different microstructure. In Figure 5, a single ordinate value (at a given W_0 and temperature) implies a dominant peak q_m and the presence of a single microstructure. Two ordinate values imply the presence of both q_m and q_s and a coexisting microstructure. Every system that has $W_0 \geq 90$ experiences some form of transition from one microstructure to another. This transition is evidenced either by the emergence of the secondary peak or by the shift from the initial dominant peak to a final dominant peak that occurs at a higher q value. The observation that the translation in the dominant-peak position is the same for any system that undergoes this transition lends further support to the idea that for any W_0 there are only two possible microstructures present that are dependent upon water content and temperature and that there exists a coexistence phase present that has components of both microstructural types (i.e., the two-peak SANS profiles). Each SANS experiment took 2−3 h at each temperature stage to complete; therefore, these coexistence phases are observable and stable. Data in Figure 5 and Table 2 also demonstrate that the trend in the transition temperatures for systems entering the coexistence region is dependent on W_0. It is observed that as W_0 increases the transition temperature decreases.

While we have proposed the 2-D hexagonal and lamellar geometries as representative of the microstructures, it is difficult to exclude other geometries conclusively with at most three peaks clearly evident in the scattering patterns. The absence of additional strong reflections from sym-

(20) Kotlarchyk, M.; Huang, J. S.; Chen, S.-H. *J. Phys. Chem.* **1985**, *89*, 4382.

metry along the "c"-axis may be one indication of 2-D geometry. In a hexagonal close-packed system of spheres, one would expect to see the strong reflections from the [101] and [002] planes. The ability of the model to predict the entire scattering patterns with temperature and water content is another verification factor. If, for example, we assume the lattice structure to be hexagonal close-packed system of spheres, we can derive the equivalent expression

$$\frac{r_t - r_w}{a} = \frac{d_s}{a} = 1.105(\sqrt[3]{\varphi_w + \varphi_s} - \sqrt[3]{\varphi_w}) \qquad (10)$$

With the same d_s and the volume fractions based on the effective density of 2.2 g/mL as shown in Table 1, the calculated q_m values for [100] reflections will not match the experimental data, although the trend with W_0 will be similar. For example, for $W_0 = 90$, the calculated value of a is 110.9 Å, and the calculated q_m is 0.033 Å^{-1}, which is below the experimental q_m of 0.043. While the hexagonal close-packed system of spheres cannot account for the scattering patterns, we do not claim that the columnar hexagonal geometry proposed implies smooth cylinders. An undulating surface roughly equivalent to a string of beads could, in principle, show similar scattering patterns that indicate a lack of multiple strong Bragg reflections.

An interesting aspect to be considered is the nature of scattering that accounts for the strong primary peak (the [1,0] reflection in the 2-D hexagonal symmetry structure) and the weak higher-order peak (the [1,1] reflection). For a 2-D hexagonal lattice where the cylinders are oriented at an angle α to the scattering vector, the integrated scattering intensity for a reflection of order hk that corresponds to q is related to the structure factor $|F^2|$ through the expression[16,21]

$$I_{q,\alpha} \propto |F_{q,\alpha}{}^2| = f_{q,\alpha}{}^2 \qquad (11)$$

where $f_{q,\alpha}$ is the intraparticle form factor. Thus,

$$\frac{I_{q_m,\alpha}}{I_{q_{ho},\alpha}} = \left(\frac{f_{q_m,\alpha}}{f_{q_{ho},\alpha}}\right)^2 \qquad (12)$$

For the case of hexagonally packed cylinders with the angle between the cylinder axis and the scattering vector equal to 90°, the ratio of the form factors can be expressed as[21]

$$\frac{I_{q_m}}{I_{q_{ho}}} = \left[\frac{J_1(q_m r_w)/(q_m r_w)}{J_1(q_{ho} r_w)/(q_{ho} r_w)}\right]^2 \qquad (13)$$

where J_1 is the Bessel function of the first kind, r_w is the radius of the water pool, and q_m and q_{ho} are the values of q for the primary and higher-order Bragg peaks corresponding to the [1,0] and [1,1] reflections, respectively. The radius of the water pool r_w is calculated from eq 4. The experimental intensity ratios for the primary and higher-order peaks are obtained by fitting the data around each peak to the sum of a Gaussian and a straight line (five parameter nonlinear least-squares fitting) and calculating the area under the Gaussian. Calculations of the intensity ratios from eq 13 are compared to the experimental values in Table 4. While the numbers are not identical, they are reasonably close to each other, lending additional credibility to the presence of the columnar hexagonal structure.

(21) Guinier, A.; Fournet, G. *Small-Angle Scattering of X-rays*; Wiley & Sons: New York, 1955.

Table 4. Comparison of Experimental and Predicted Intensity Ratios for the Primary and Higher-Order Peaks for a Columnar Hexagonal Structure

W_0	T (°C)	experimental intensity ratio	calculated intensity ratio
90	25	10.61 ± 0.05	6.8
90	38	11.33 ± 0.07	6.9
110	25	5.05 ± 0.17	4.4
110	38	5.45 ± 0.23	4.5

A mechanism for this transition from the hexagonal to the lamellar phase as described in Figure 6 is proposed. The initial microstructure is hexagonal, with one dominant peak representative of the [1,0] spacings, d_h, present in the SANS profile. Although this microstructure is shown (and modeled) as hexagonally arranged cylinders with a circular cross section, it is quite possible that a nonuniform surfactant distribution may result in cross sections of varying geometry, with AOT preferentially occupying regions of higher curvature. The amphiphilic layer that forms the hexagonally arranged columns is then deformed and elongated by an increase in temperature or water content. As either variable is increased further, a coexistence region containing the two different phases with unique length scales d_h and d_l is induced. The coexistence region has to be stable to be measured as a SANS spectrum. This stability leads to the emergence of the two peaks present in the SANS data and is essential for this transition to occur. Finally, at progressively higher temperatures, a lamellar microstructure is formed, and only one length scale, d_l, is present. Similar phase-transition behavior (temperature-induced transitions from the hexagonal to the lamellar structure) has been noted recently in a four-component polymer + surfactant system.[22]

Figure 7 presents a summary of the connection between W_0, temperature, and the microstructure of the gel phase. As W_0 increases, it is observed that the transition temperature (T) for entry into the coexistence region decreases and that this trend appears to be somewhat diagonal across the compositions and temperatures analyzed. This process is also completely thermally reversible, as shown by the agreement in the final and initial data for all of the systems listed in Table 2.

The presence of the well-defined primary peaks implies the existence of long-range order in the gels and provides an opportunity for calculation of the average size of the domains responsible for the scattering, d_{domain}, using the Scherrer relationship:[23]

$$d_{domain} = 0.94\,\lambda/(\Delta 2\theta_{domain} \cos\theta) \qquad (14)$$

Here, λ is the wavelength of the incident neutrons, θ is the scattering angle, and $\Delta 2\theta_{domain}$ is the spread in the scattering angle caused by the finite size of the domains. To a first approximation,

$$\Delta 2\theta_{domain} = [(\Delta 2\theta_{measured})^2 - (\Delta 2\theta_{instrument})^2]^{1/2} \qquad (15)$$

where $\Delta 2\theta_{measured}$ is the experimentally observed full width at half-maximum (fwhm) for the primary peak and $\Delta 2\theta_{instrument}$ is the instrument resolution. The instrument resolution is dictated by a variety of factors, including the spread in the incident wavelength, the finite size of the

(22) Firestone, M. A.; Thiyagarajan, P.; Tiede, D. M. *Langmuir* **1998**, *14*, 4688.

(23) Warren, B. E. *X-ray Diffraction*; Addison-Wesley: Reading, MA, 1969.

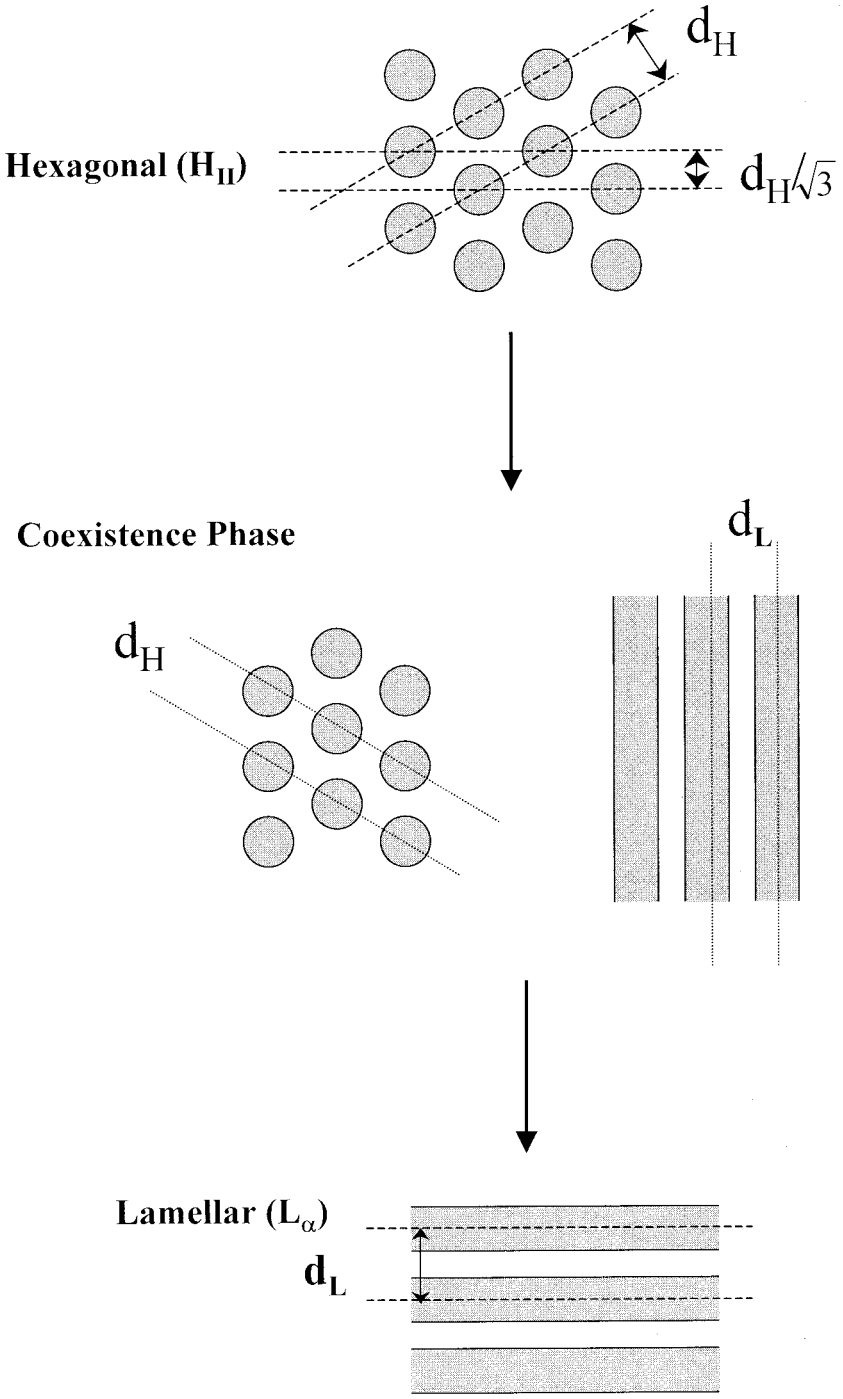

Figure 6. Schematic depicting the transition from hexagonal to lamellar microstructures illustrating the characteristic *d*-spacings for each geometry.

beam, and the resolution of the array detector. The spread in q (Δq) at each scattering angle is a part of the data set recorded during any experimental run and is used directly in these calculations. The relationship between the magnitude of the scattering vector q and the scattering angle θ provides the connection between Δq and $\Delta 2\theta_{\text{instrument}}$. Excluding the transition phases, the domain sizes calculated range from 70 to 120 nm, implying that there are approximately 4−8 unit cells across a single domain.

Finally, we bring out the interesting feature of an increase in scattering intensity at q values smaller than the primary peak. Additional SANS experiments with $q \leq 0.004$ Å^{-1} show no evidence of a peak. With increasing water content, this increase in scattering intensity at low q becomes more pronounced. Scattering at very low q indicates the presence of structures characterized by very long correlation lengths that are possibly due to some interaction between and subsequent ordering of lamellar domains. Further study is required to elucidate the origins of this intensity.

Conclusions

The microstructure of a surfactant-based rigid gel mesophase has been investigated with SANS. The scattering patterns are consistent with interpretations of the microstructure as columnar hexagonal or lamellar. Increasing the water content or the temperature drives transitions from columnar hexagonal microstructures to lamellar microstructures. The models for columnar hexagonal and lamellar geometries represent the scattering

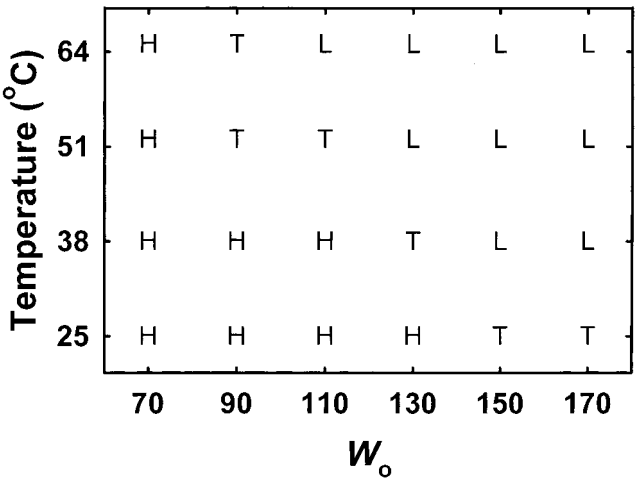

Figure 7. Plot of W_0 vs temperature demonstrating the trends present in the microstructural transformation. H denotes the inverted hexagonal microstructure (H_{II}), T denotes the transition stage of coexisting microstructures, and L denotes the lamellar microstructure (L_α).

patterns very consistently. The clarity with which SANS describes the microstructures and allows the capture of coexisting structures in this system is rather notable. Through SANS, we are able not only to identify microstructures but also to quantify the characteristic dimensions of these microstructures.

Knowledge of these crystalline microstructures with surfactant systems could have many applications in materials synthesis. Surfactant solutions and lyotropic liquid crystalline systems are of significant interest in templating the synthesis of nanostructured materials.[24−26] The biomimetic synthesis of extended ceramic structures has also been explored using surfactant systems.[27] Recently, the use of small molecules to gelate organic solvents has been of interest because of potential applications to structured materials synthesis.[28−30] The surfactant microstructures described here fall into the category of systems in which aqueous-phase synthesis may be combined with organic-phase synthesis to create functional nanocomposites. The ability to selectively modify the microstructure through composition or temperature may also be of benefit in directing the morphological synthesis of materials.

The synergistic effect of the two surfactants in forming the gel phase is also of interest Possible applications include the design of specific gel microstructures by combining surfactants with different packing parameters. The phase stability of the gel over a range of surfactant compositions and the characteristics of the gel's microstructure are continuing research efforts.

Acknowledgment. We are grateful to Dr. Boualem Hammouda (NIST) and Dr. Anthony Nunes (University of Rhode Island) for very helpful discussions. Dr. Hammouda is also acknowledged for help in acquiring the SANS data. The National Institute of Standards and Technology, U.S. Department of Commerce, is gratefully acknowledged for providing both the neutron research facilities and funding (Grant NSF/DMR-9986442) for this work. Additional financial support was obtained from the National Science Foundation (Grants 9909912 and 990195) and DARPA/AMRI (Grant No MDA 972-97-1-0003). NIST does not endorse equipment or chemicals mentioned in this work.

LA011530R

(24) Lee, Y.-S.; Jian-Zhong Yang, J.-Z.; Sission, T. M.; Frankel, D. A.; Gleeson, J. T.; Aksay, E.; Keller, S. L.; Gruner, S. M.; O'Brien, D. F. *J. Am. Chem. Soc.* **1995**, *117*, 5573.
(25) Pileni, M. P. *Langmuir* **1997**, *13*, 3266.
(26) Pavel, F. M.; Mackay, R. A. *Langmuir* **2000**, *16*, 8568.
(27) Mann, S.; Burkett, S.; Davis, S.; Fowler, C.; Mendelson, N.; Simms, S.; Walsh, D.; Whilton, N. *Chem. Mater.* **1997**, *9*, 2300.
(28) Abdallah, D. J.; Weiss, R. G. *Adv. Mater. (Weinheim, Ger.)* **2000**, *12*, 1237. Terech, P.; Ostuni, E.; Weiss, R. G. *J. Phys. Chem.* **1996**, *100*, 3759.
(29) Geiger, C.; Stanescu, M.; Chen, L.; Whitten, D. G. *Langmuir* **1999**, *15*, 2241. Wang, R.; Geiger, C.; Chen, L.; Swanson, B.; Whitten, D. G. *J. Am. Chem. Soc.* **2000**, *122*, 2399.
(30) Jung, J. H.; Ono, Y.; Seiji, S. *Chem.—Eur. J.* **2000**, *6*, 4552. de Loos, M.; van Esch, J.; Stokroos, I.; Kellogg, R. M.; Feringa, B. L. *J. Am. Chem. Soc.* **1997**, *119*, 12675.